PERGAMON

International Journal of Solids and Structures 38 (2001) 2803–2820

INTERNATIONAL JOURNAL OF SOLIDS and STRUCTURES

www.elsevier.com/locate/ijsolstr

Modelling and analysis of dynamic interaction between piezoelectric actuators

X.D. Wang [1], S.A. Meguid *

Department of Mechanical and Industrial Engineering, Engineering Mechanics and Design Laboratory, University of Toronto, 5 King's College Road, Toronto, Ont., Canada M5S 3G8

Received 6 February 1999; in revised form 23 April 2000

Abstract

This article provides a comprehensive theoretical treatment of the coupled dynamic electromechanical behaviour of interacting piezoceramic actuators embedded in an elastic medium under inplane electrical load. The actuators are characterized by an electroelastic line model with the poling direction being perpendicular to its length. The theoretical formulations, governing this coupled system, are based upon the use of integral equations and a new pseudo-incident wave method. A new shear stress singularity factor (SSSF) at the tip of the actuator is obtained by solving these integral equations using Chebyshev polynomial expansions. Typical examples are provided to show the effect of the geometry of the actuator, the material combination and the loading frequency upon the SSSF.

Keywords: Dynamics; Piezoelectric; Actuator; Interaction

1. Introduction

With the emergence of new piezoceramic materials, the concept of using a network of piezoelectric actuators and sensors to form a self controlling and self monitoring smart system in advanced structural design has drawn considerable interest among the research community (Gandhi and Thompson, 1992; Disch et al., 1995; Varadan et al., 1993). One of the most fundamental issues surrounding the use of integrated actuators in smart material/structure systems is to determine the actuation effect being transferred from the actuators to the host structure and the resulting overall response. Another important aspect related to the design of any integrated smart system is the determination of interfacial stresses that may result in degrading the mechanical integrity of the structure. An accurate assessment of the coupled electromechanical behaviour of an integrated structure would require the determination of the local stress distribution in smart structures involving piezoelectric actuators/inhomogeneities.

* Corresponding author. Tel.: +1-416-978-5741; fax: +1-416-978-7753.
E-mail address: meguid@mie.utoronto.ca (S.A. Meguid).
[1] Present address: Department of Mechanical Engineering, University of Alberta, Edmonton, Alberta, Canada T6G 2G8.

0020-7683/01/$ - see front matter
PII: S0020-7683(00)00183-9

The subject of piezoelectric actuator/inhomogeneity has received attention from the scientific community. For example, Deeg (1980) and Benveniste (1992) conducted research on the single elliptical (ellipsoidal) inhomogeneity in unbounded piezoelectric materials using Green's function approach; Dunn and Taya (1993) focused on the determination of the effective properties of piezoelectric composites using different micromechanical models; and the work of Pak (1990), Sosa (1991), Suo et al. (1992), Jain and Sirkis (1994) and He et al. (1994) on fracture and damage analysis of piezoceramics. However, relatively few studies have focused on the local stress field around piezoelectric actuators. Crawley and de Luis (1987) first analysed a beam-like structure with surface bonded and embedded thin sheet piezoelectric actuators to study the stresses transferred by the actuator to the host beam. In that analysis, the axial stress in the actuator was assumed to be uniform across its thickness and the host structure was treated as a Bernoulli–Euler beam. The result indicated that for a perfectly bonded actuator, the shear stress between the actuator and the host beam was transferred over an infinitesimal distance near the ends of the actuator. Crawley and Anderson (1990) further developed a Bernoulli–Euler model of a piezoelectric actuator by considering the linear stress distribution along its thickness.

Im and Atluri (1989) modified the actuator model presented by Crawley and de Luis (1987) to investigate a beam with a piezoelectric actuator under general loading. Both the axial and the transverse shear forces in the beam were considered in formulating the governing equations. A refined actuator model based on the plane stress condition was presented for a beam structure with symmetrically surface-bonded actuator patches (Lin and Rogers, 1993a,b), which showed good agreement with the finite element results.

The objective of the present paper is to provide an analytical analysis of the coupled dynamic electromechanical behaviour of interacting piezoceramic actuators embedded in an elastic medium under inplane mechanical and electrical loads. Since the main interest of the current study is the local stress concentration and the load transfer near the actuator, the host structure is assumed to be infinite.

The single actuator problem was solved using one-dimensional actuator model and solving the resulting integral equations in terms of the interfacial shear stress. The single actuator solution was further implemented into a new pseudo-incident wave method to account for the dynamic interaction between actuators. Specifically, two aspects of the work were examined. The first was concerned with determining the effect of the geometry, the material mismatch and the loading frequency upon the resulting shear stress singularity factor (SSSF), while the second was concerned with the effect of the interaction between actuators upon the local stress field around the actuators.

2. Formulation of the problem

2.1. General description

Let us consider a two-dimensional linear elastic solid with multiple parallel piezoelectric actuators A_n ($n = 1, N_a$) under plane strain condition, as shown in Fig. 1. The matrix is assumed to be an insulator and perfectly bonded to the actuators. Each actuator A_n is subjected to an applied electric field (E_n) of frequency ω across its thickness. The position of the centre of actuator A_n is described by its coordinates (y_n^0, z_n^0), and its half length and the thickness are denoted as a_n and h_n, respectively. A local coordinate system (y_n, z_n) will be used to describe actuator A_n with its origin at the centre of A_n.

The displacement, strain, stress and electric fields corresponding to a steady state solution under a dynamic load of frequency ω can be expressed in terms of the frequency ω as

$$A^{\mathrm{f}}(y,z,t) = A(y,z)\mathrm{e}^{-\mathrm{i}\omega t}, \tag{1}$$

where A^{f} represents the desired field variable. For the sake of convenience, the time factor $\exp(-\mathrm{i}\omega t)$ will be suppressed and only $A(x,y)$ will be considered. It is further assumed that the system considered is under plane strain deformation, which corresponds to the case where the structure is relatively large in size in the

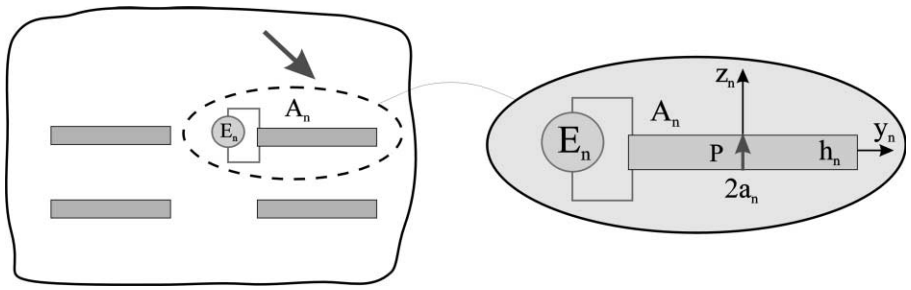

Fig. 1. A composite structure with embedded actuators.

direction perpendicular to the working plane. It should be mentioned that the current method and solution could also be applied to plane stress cases by the appropriate substitution of the material constants.

As in most of the thin sheet piezoelectric actuator applications, it is assumed that the poling direction of a piezoelectric actuator is perpendicular to its length and that the two electrodes are attached to the upper and the lower surfaces of the actuator, respectively. The electric field is induced by applying a voltage (V_n) across the upper and lower electrodes, which can be determined using $E_n = (V_n^- - V_n^+)/h_n$.

For thin actuators, the applied electric field will mainly result in an axial deformation, and the following assumptions can be made:

(1) σ_y^a and u_y^a are uniform across the thickness of the actuator,
(2) the interfacial shear stress (τ) transferred between the actuator and the host can be replaced by a distributed body force along the actuator, and
(3) σ_z^a and σ_{yz}^a in the actuator can be ignored.

Based upon these assumptions, the actuator can be modelled as an electroelastic line subjected to the applied electric field and distributed axial force, τ/h, as shown in Fig. 2. The equilibrium equation of the actuator can then be expressed as

$$\frac{d\sigma_y^a}{dy} + \tau(y)/h + \rho_a \omega^2 u_y^a = 0, \tag{2}$$

where ρ_a is the mass density of the actuator. The relation between the stress, the strain and the electric fields of this actuator model can be obtained by using the following general constitutive relation:

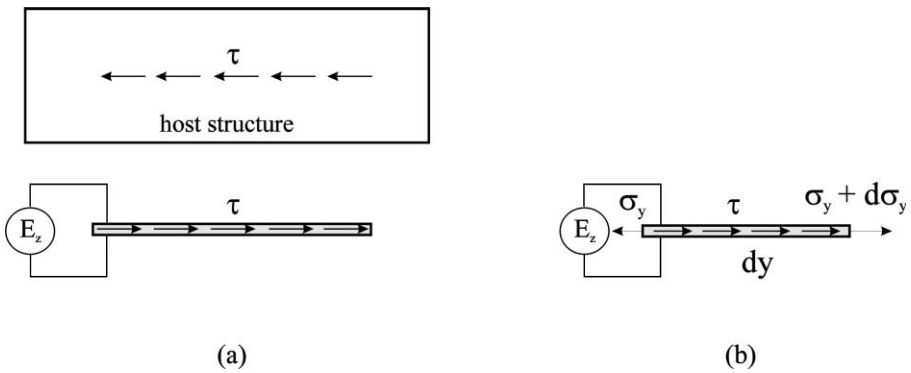

Fig. 2. Actuator model.

$$\sigma_y^{\mathrm{a}} = E_{\mathrm{a}}\epsilon_y^{\mathrm{a}} - e_{\mathrm{a}}E_z, \tag{3}$$

where $\epsilon_y^{\mathrm{a}} = \partial u_y^{\mathrm{a}}/\partial y$ is the axial strain of the actuator and E_{a} and e_{a} are effective material constants given in Appendix A.

The elastodynamic behaviour of the homogeneous isotropic matrix under steady state plane strain deformation is governed by the following equations (Achenbach, 1973),

$$(\nabla^2 + K^2)\Phi = 0, \qquad (\nabla^2 + k^2)\Psi = 0 \tag{4}$$

in which the Laplacian operator ∇^2 stands for $(\partial^2/\partial y^2) + (\partial^2/\partial z^2)$, Φ and Ψ are two displacement potentials and K and k are two wave numbers defined as

$$K = \omega/c_{\mathrm{L}}, \quad k = \omega/c_{\mathrm{T}} \tag{5}$$

with c_{L} and c_{T} being the longitudinal and transverse shear wave velocities of the elastic medium, respectively. The non-vanishing displacement components are

$$u_y = \frac{\partial\Phi}{\partial y} + \frac{\partial\Psi}{\partial z}, \qquad u_z = \frac{\partial\Phi}{\partial z} - \frac{\partial\Psi}{\partial y}. \tag{6}$$

The corresponding strain and stress components are

$$\epsilon_y = \frac{\partial u_y}{\partial y}, \quad \epsilon_z = \frac{\partial u_z}{\partial z}, \quad \epsilon_{yz} = \frac{1}{2}\left(\frac{\partial u_z}{\partial y} + \frac{\partial u_y}{\partial z}\right) \tag{7}$$

and

$$\begin{cases} \sigma_y = \mu\left[-k^2\Phi - 2\frac{\partial^2\Phi}{\partial z^2} + 2\frac{\partial^2\Psi}{\partial y\partial z}\right], \\ \sigma_z = \mu\left[-k^2\Phi - 2\frac{\partial^2\Phi}{\partial y^2} - 2\frac{\partial^2\Psi}{\partial y\partial z}\right], \\ \sigma_{yz} = \mu\left[2\frac{\partial^2\Phi}{\partial y\partial z} - k^2\Psi - 2\frac{\partial^2\Psi}{\partial y^2}\right], \end{cases} \tag{8}$$

where μ is the shear modulus of the elastic medium.

3. Analysis of a single piezoelectric actuator

Let us now consider the plane strain problem of a thin piezoceramic actuator sheet embedded in a homogeneous and isotropic elastic medium. The half length and the thickness of the actuator are denoted as a and h, respectively, as shown in Fig. 3. It is assumed that the poling direction of the actuator is along the z-axis.

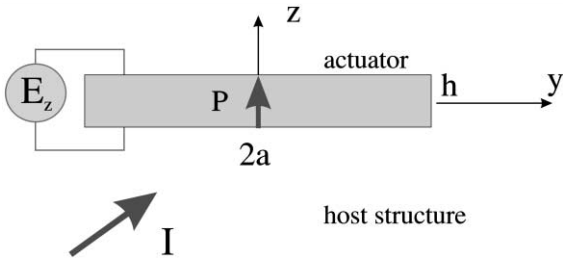

Fig. 3. An embedded actuator.

3.1. Displacement of the actuator

Eq. (2) can be formulated, using Eq. (3), in terms of the axial displacement of the actuator as follows:

$$E_a \frac{\mathrm{d}^2 u_y^{\mathrm{a}}}{\mathrm{d}y^2} + F(y)/h + \rho_{\mathrm{a}}\omega^2 u_y^{\mathrm{a}} = 0, \tag{9}$$

where

$$F(y) = \tau(y) - h e_{\mathrm{a}} \frac{\mathrm{d}E_z(y)}{\mathrm{d}y} \tag{10}$$

is the applied electromechanical load with τ being the interfacial shear stress along the actuator, as shown in Fig. 2. Since all the load transfer between the actuator and the host can be attributed to τ, the two ends of the actuator can be assumed to be traction free, i.e.

$$\sigma_y^{\mathrm{a}} = 0, \quad |y| = a. \tag{11}$$

By solving the second order differential equation (9), and making use of the boundary conditions given by Eq. (11), the axial displacement of the actuator for a general applied τ can be obtained as

$$u_y^{\mathrm{a}}(y) = f_E(y) - \frac{\cos k_{\mathrm{a}}(a+y)}{h k_{\mathrm{a}} E_{\mathrm{a}} \sin 2k_{\mathrm{a}} a} \int_{-a}^{a} \cos k_{\mathrm{a}}(\xi - a)\tau(\xi)\mathrm{d}\xi + \int_{-a}^{y} \sin k_{\mathrm{a}}(\xi - y) \frac{\tau(\xi)}{h k_{\mathrm{a}} E_{\mathrm{a}}} \mathrm{d}\xi, \tag{12}$$

where

$$k_{\mathrm{a}} = \omega/c_{\mathrm{a}}, \quad \text{and} \quad c_{\mathrm{a}} = \sqrt{E_{\mathrm{a}}/\rho_{\mathrm{a}}} \tag{13}$$

are the wave number and the axial wave speed of the actuator, respectively. The axial displacement induced by a uniformly applied electric field, E_z, is given by

$$f_E(y) = \frac{E_z e_{\mathrm{a}}}{E_{\mathrm{a}} k_{\mathrm{a}}} \frac{\sin k_{\mathrm{a}} y}{\cos k_{\mathrm{a}} a}. \tag{14}$$

3.2. Displacement field in the matrix

The dynamic displacement and stress fields in the elastic matrix can be decomposed into two parts: incident and outgoing ones, as shown in Fig. 4. The total stress and displacement fields in the matrix $(\sigma_{ij}^{\mathrm{T}}, u_j^{\mathrm{T}})$ can then be expressed as the superposition of the incident wave $(\sigma_{ij}^{\mathrm{I}}, u_j^{\mathrm{I}})$ and the induced wave (σ_{ij}, u_j), i.e.,

$$\sigma_{ij}^{\mathrm{T}} = \sigma_{ij}^{\mathrm{I}} + \sigma_{ij}, \qquad u_j^{\mathrm{T}} = u_j^{\mathrm{I}} + u_j \tag{15}$$

with the superscripts 'T' and 'I' representing the total field and the incident field, respectively.

The outgoing wave can be determined by solving the governing equations given by Eq. (4) using the following Fourier transform:

$$f^*(s) = \frac{1}{2\pi} \int_{-\infty}^{\infty} f(y) \mathrm{e}^{\mathrm{i}sy} \mathrm{d}y, \qquad f(y) = \int_{-\infty}^{\infty} f^*(s) \mathrm{e}^{-\mathrm{i}sy} \mathrm{d}s \tag{16}$$

as

$$\begin{cases} \Phi_+^*(s,z) = A^+(s)\mathrm{e}^{-\alpha z}, & \Psi_+^*(s,z) = B^+(s)\mathrm{e}^{-\beta z} \qquad z > 0, \\ \Phi_-^*(s,z) = A^-(s)\mathrm{e}^{\alpha z}, & \Psi_-^*(s,z) = B^-(s)\mathrm{e}^{\beta z} \qquad z < 0, \end{cases} \tag{17}$$

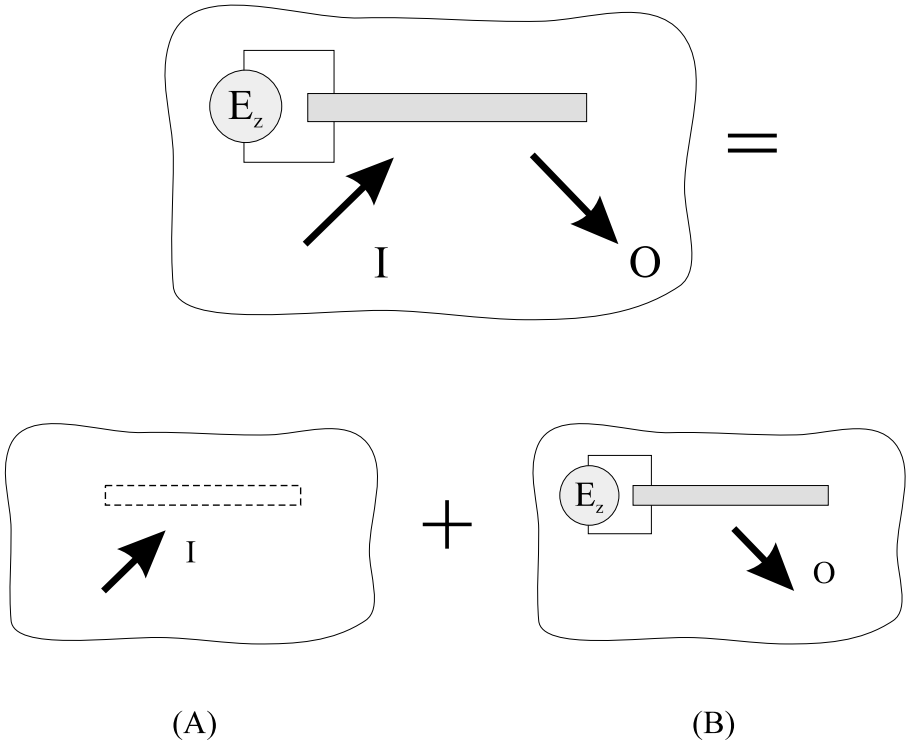

Fig. 4. Decomposition of the problem.

where $(^*)$ represents Fourier transform. $A^+(s)$, $B^+(s)$, $A^-(s)$ and $B^-(s)$ are four unknown functions of s with α and β being given by

$$\alpha = \begin{cases} \sqrt{s^2 - K^2}, & |s| > K, \\ -\mathrm{i}\sqrt{K^2 - s^2}, & |s| < K, \end{cases} \qquad \beta = \begin{cases} \sqrt{s^2 - k^2}, & |s| > k, \\ -\mathrm{i}\sqrt{k^2 - s^2}, & |s| < k, \end{cases} \tag{18}$$

which ensure that the stress field induced by the outgoing wave satisfies the boundary conditions of the problem at infinity.

According to the solution given by Eq. (17), the following displacement and stress expressions can be obtained by using Eqs. (6) and (8):

$$u_y^* = \begin{cases} -\mathrm{i}sA^+(s)\mathrm{e}^{-\alpha z} - \beta B^+(s)\mathrm{e}^{-\beta z}, & z > 0, \\ -\mathrm{i}sA^-(s)\mathrm{e}^{\alpha z} + \beta B^-(s)\mathrm{e}^{\beta z}, & z < 0, \end{cases} \tag{19}$$

$$\sigma_{yz}^* = \mu \begin{cases} 2\mathrm{i}s\alpha A^+(s)\mathrm{e}^{-\alpha z} + (2s^2 - k^2)B^+(s)\mathrm{e}^{-\beta z}, & z > 0, \\ -2\mathrm{i}s\alpha A^-(s)\mathrm{e}^{-\alpha z} + (2s^2 - k^2)B^-(s)\mathrm{e}^{-\beta z}, & z < 0. \end{cases} \tag{20}$$

According to the present actuator model, the displacement field of the induced wave should be continuous at the site of the actuator. Therefore, the Fourier transform of this displacement should satisfy the following conditions:

$$u_y^*(s, 0^+) = u_y^*(s, 0^-). \tag{21}$$

The shear stress of the outgoing wave at the upper and the lower surfaces of the actuator are discontinuous. The mismatch stress can be expressed in the Fourier transform domain as

$$\tau^* = \sigma^*_{yz}(s,0^+) - \sigma^*_{yz}(s,0^-). \tag{22}$$

By making use of Eqs. (21) and (22), the unknown functions A^+, A^-, B^+ and B^- can be obtained in terms of τ^*, such that

$$\begin{cases} A^+ = A^- = -\frac{1}{2\mu k^2}\frac{\mathrm{i}s}{\alpha}\tau^*(s), \\ B^+ = -B^- = -\frac{1}{2\mu k^2}\tau^*(s). \end{cases} \tag{23}$$

By substituting Eq. (23) into Eq. (19) and making use of inverse Fourier transform, the displacement at $z = 0$ can be expressed in terms of τ^* as

$$u_y(y,0) = \frac{1}{2\mu k^2}\int_{-\infty}^{\infty}\left(\beta - \frac{s^2}{\alpha}\right)\tau^*(s)\mathrm{e}^{-\mathrm{i}sy}\,\mathrm{d}s. \tag{24}$$

Since the shear stress σ_{yz} is continuous in $|y| > a$, $z = 0$, according to Eq. (22), the mismatch shear stress $\sigma_{yz}(y,0^+) - \sigma_{yz}(y,0^-)$ must be zero at $|y| > a$. For $|y| < a$, however, the mismatch shear stress equals the interfacial shear stress τ used in Eq. (10). Accordingly, τ^* can be expressed in terms of τ as

$$\tau^*(s) = \frac{1}{2\pi}\int_{-a}^{a}\tau(\xi)\mathrm{e}^{\mathrm{i}s\xi}\,\mathrm{d}\xi. \tag{25}$$

The displacement at $z = 0$ can then be expressed, by substituting Eq. (25) into Eq. (24), as

$$u_y(y,0) = \frac{1}{2\pi\mu}\int_{-a}^{a}\tau(\xi)n_1(y-\xi)\mathrm{d}\xi, \tag{26}$$

where

$$n_1(y-\xi) = \frac{1}{k^2}\int_0^{\infty}\left[\beta - \frac{s^2}{\alpha}\right]\cos[s(\xi - y)]\mathrm{d}s. \tag{27}$$

3.3. Continuity conditions and integral equations

The continuity condition between the actuator and the matrix can be described, using Eq. (15), as being

$$u^{\mathrm{a}}_y = u_y + u^{\mathrm{I}}_y \tag{28}$$

with the superscripts 'a' and 'I' representing the actuator and the incident wave, respectively. By substituting Eqs. (26) and (12) into Eqs. (28), the following integral equation can be obtained for τ:

$$\begin{aligned} &\frac{1}{2\pi\mu}\int_{-a}^{a}\tau(\xi)n_1(y-\xi)\mathrm{d}\xi + \frac{\cos k_{\mathrm{a}}(a+y)}{k_{\mathrm{a}}\sin 2k_{\mathrm{a}}a}\int_{-a}^{a}\cos k_{\mathrm{a}}(\xi - a)\frac{\tau(\xi)}{hE_{\mathrm{a}}}\mathrm{d}u - \int_{-a}^{y}\sin k_{\mathrm{a}}(\xi - y)\frac{\tau(\xi)}{hk_{\mathrm{a}}E_{\mathrm{a}}}\mathrm{d}\xi \\ &\quad = f_E(y) - u^{\mathrm{I}}_y, \quad |y| < a, \end{aligned} \tag{29}$$

where u^{I}_y is the displacement of the incident field, which represents the applied mechanical load, and f_E is the electrical load given by Eq. (14).

Eq. (29) can be normalised as

$$\frac{\overline{k}_a}{2(1-\nu)\overline{k}_a^2}\int_{-1}^{1}\overline{\tau}(\zeta)\int_0^{\infty}\left(\overline{\beta}-\frac{\overline{s}^2}{\overline{\alpha}}\right)\cos[\overline{s}(\eta-\zeta)]\mathrm{d}s\,\mathrm{d}\zeta+q\frac{\cos[\overline{k_a}(\eta+1)]}{\sin(2\overline{k}_a)}\int_{-1}^{1}\cos\overline{k}_a(\zeta-1)\overline{\tau}(\zeta)\mathrm{d}\zeta$$
$$-q\int_{-1}^{\eta}\sin\overline{k}_a(\zeta-\eta)\overline{\tau}(\zeta)\mathrm{d}\zeta=\frac{E_ak_a}{e_aE_z}f_E(y)-\frac{E_ak_a}{e_aE_z}u_y^{\mathrm{I}},\quad|\eta|<1. \tag{30}$$

The normalised parameters in these equations are defined by

$$\overline{\tau}(\eta)=\tau(a\eta)/p,\qquad\overline{\phi}_m(\eta)=\phi_m(a\eta),\qquad\eta=y/a, \tag{31}$$

$$\overline{K}=Ka,\quad\overline{k}=ka,\quad\overline{k_a}=k_aa, \tag{32}$$

$$q=\frac{\pi\mu a}{(1-\nu)E_ah},\qquad p=\frac{\pi\mu e_aE_z}{(1-\nu)E_a}. \tag{33}$$

3.4. Solution of the problem

Eq. (30) involves a square-root singularity of $\overline{\tau}$ at the ends of the actuators. Therefore, the general solution of $\overline{\tau}$ can be expressed in terms of Chebyshev polynomials, such that

$$\overline{\tau}(\eta)=\sum_{j=0}^{\infty}c_jT_j(\eta)/\sqrt{1-\eta^2}. \tag{34}$$

By substituting Eq. (34) into Eq. (30) and making use of the following relations:

$$\begin{cases}\int_{-1}^{1}\frac{1}{\sqrt{1-\zeta^2}}T_j(\zeta)\sin(\overline{s}\zeta)\mathrm{d}\zeta=\begin{cases}0, & j=2n,\\(-1)^n\pi J_j(\overline{s}), & j=2n+1,\end{cases}\\ \int_{-1}^{1}\frac{1}{\sqrt{1-\zeta^2}}T_j(\zeta)\cos(\overline{s}\zeta)\mathrm{d}\zeta=\begin{cases}0, & j=2n+1,\\(-1)^n\pi J_j(\overline{s}), & j=2n,\end{cases}\end{cases} \tag{35}$$

the following algebraic equations for determining c_j can be obtained,

$$\frac{\pi\overline{k}_a}{2(1-\nu)\overline{k}_a^2}\sum_{j=0}^{\infty}c_j\int_0^{\infty}P_j^1(\overline{s},\eta)\left(\overline{\beta}-\frac{\overline{s}^2}{\overline{\alpha}}\right)\mathrm{d}\overline{s}-qv\sum_{j=0}^{\infty}c_j\int_{\cos^{-1}\eta}^{\pi}\sin[\overline{k_a}(\cos\theta-\eta)]\cos(j\theta)\mathrm{d}\theta+qv$$
$$\times\frac{\cos[\overline{k}_a(\eta+1)]}{\sin(2\overline{k}_a)}\sum_{j=0}^{\infty}c_jP_j^2=\frac{E_ak_a}{e_aE_z}f_E(a\eta)-\frac{E_ak_a}{e_aE_z}u_y^{\mathrm{I}}(a\eta),\quad|\eta|<1, \tag{36}$$

where

$$\begin{cases}P_j^1(\overline{s},\eta)=J_j(\overline{s})\begin{cases}(-1)^n\cos(\overline{s}\eta), & j=2n,\\(-1)^n\sin(\overline{s}\eta), & j=2n+1,\end{cases}\\ P_j^2=J_j(\overline{k}_a)\begin{cases}(-1)^n\sin(\overline{k}_a), & j=2n+1,\\(-1)^n\cos(\overline{k}_a), & j=2n\end{cases}\end{cases} \tag{37}$$

with J_j $(j=1,2,\ldots)$ being Bessel functions of the first kind.

If the expansions in Eq. (34) are truncated to the $(N-1)$th term and Eq. (36) is satisfied at the following collocation points along the length of the actuator

$$\eta^l=\cos\left[\frac{l-1}{N-1}\pi\right],\quad l=1,2,\ldots,N, \tag{38}$$

N linear algebraic equations in terms of $\{c\}=\{c_0,c_1,c_2,\ldots,c_{N-1}\}^{\mathrm{T}}$ can be obtained, such that

$$[A]\{c\} = \{F\}, \tag{39}$$

where $[A]$ is a known matrix given in Appendix B and $\{F\}$ is the applied load with

$$F_l = \frac{E_a k_a}{e_a E_z} f_E(a\eta^l) - \frac{E_a k_a}{e_a E_z} u_y^{\mathrm{I}}(a\eta^l), \quad l = 1, 2, \ldots, N. \tag{40}$$

From these equations, the unknown coefficients in $\{c\}$ can be determined.

The outgoing wave in the matrix medium is governed by interfacial stress τ. By making use of Eqs. (6), (17) and (23), the outgoing displacement field in the matrix can be obtained in terms of τ as

$$\begin{cases} u_y^+ = \frac{1}{2\pi\mu k^2} \int_0^\infty [-\frac{s^2}{\alpha} e^{-\alpha z} + \beta e^{-\beta z}] \int_{-a}^{a} \tau(\xi) \cos[s(\xi - y)] d\xi\, ds, \\ u_y^- = \frac{1}{2\pi\mu k^2} \int_0^\infty [-\frac{s^2}{\alpha} e^{\alpha z} + \beta e^{\beta z}] \int_{-a}^{a} \tau(\xi) \cos[s(\xi - y)] d\xi\, ds, \end{cases} \tag{41}$$

$$\begin{cases} u_z^+ = \frac{1}{2\pi\mu k^2} \int_0^\infty [-s(e^{-\alpha z} - e^{-\beta z})] \int_{-a}^{a} \tau(\xi) \cos[s(\xi - y)] d\xi\, ds, \\ u_z^- = \frac{1}{2\pi\mu k^2} \int_0^\infty [s(e^{\alpha z} - e^{\beta z})] \int_{-a}^{a} \tau(\xi) \cos[s(\xi - y)] d\xi\, ds. \end{cases} \tag{42}$$

4. Analysis of interacting actuators

The existence of multiple actuators in a smart structure subjected to dynamic loading results in complicated reflection of elastic waves between actuators. The analysis of such a complex problem can be simplified by using the previously developed single actuator solution as a building block and considering the consistency relation between different actuators. In the following discussion, $\mathbf{u} = (u_y, u_z)$ will be used to describe the displacement field in the matrix.

4.1. Pseudo-incident wave method

Let us now focus our attention on a specific actuator A_n subjected to an electric field E_n across its thickness and an incident mechanical wave $\mathbf{u}_n^{\mathrm{I}}$. $\mathbf{u}_n^{\mathrm{I}}$ includes not only the original mechanical incident wave $\mathbf{u}^0$ but also the mechanical wave from other actuators, which is regarded as an unknown pseudo-incident wave $\mathbf{u}_n^{\mathrm{p}}$, as shown in Fig. 5. Therefore, actuator A_n is subjected to an applied electric field E_n and an incident wave given by

$$\mathbf{u}_n^{\mathrm{I}} = \mathbf{u}^0 + \mathbf{u}_n^{\mathrm{p}}. \tag{43}$$

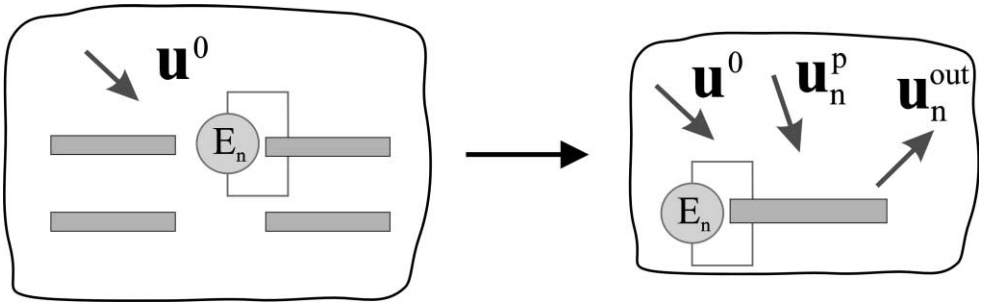

Fig. 5. Pseudo-incident waves of different actuators.

According to the single actuator solution discussed in the previous section, the applied electric field E_n and the incident wave given by Eq. (43) will result in an induced wave $\mathbf{u}_n^{\text{out}}$ in the matrix, which is given by Eqs. (41) and (42). As a result, the total displacement field in the matrix can be obtained by superimposing the incident wave and the outgoing wave as

$$\mathbf{u}^{\text{total}} = \mathbf{u}_n^{\text{I}} + \mathbf{u}_n^{\text{out}} = \mathbf{u}^0 + \mathbf{u}_n^{\text{p}} + \mathbf{u}_n^{\text{out}}. \tag{44}$$

The total displacement field in the matrix can also be obtained by summing up the initial incident field and the contribution (outgoing waves) from all actuators to give

$$\mathbf{u}^{\text{total}} = \mathbf{u}^0 + \sum_{n=1}^{N_{\text{a}}} \mathbf{u}_n^{\text{out}}. \tag{45}$$

Comparison between Eqs. (44) and (45) indicates that

$$\sum_{j=1}^{N_{\text{a}}} \mathbf{u}_j^{\text{out}} = \mathbf{u}_n^{\text{p}} + \mathbf{u}_n^{\text{out}}. \tag{46}$$

Therefore, the pseudo-incident wave of actuator n can be expressed in terms of the outgoing waves of other actuators as

$$\mathbf{u}_n^{\text{p}} = \sum_{m\neq n}^{N_{\text{a}}} \mathbf{u}_m^{\text{out}}. \tag{47}$$

Eq. (47) represents the consistency condition between different actuators. This equation will be used to solve interaction problems from single actuator solutions.

According to the single actuator solution, the outgoing wave of any actuator is governed by its interfacial shear stress, as shown in Eqs. (41) and (42). By substituting Eq. (34) into Eq. (41), the outgoing wave of actuator A_n used in Eq. (47) can be expressed in terms of the coefficients of Chebyshev polynomial expansions of actuator A_m, $\{c\}^m$, as

$$u_{y_m}^{\text{out}}(y_m, z_m) = [R_m(y_m, z_m)]\{c\}^m, \tag{48}$$

where

$$[R_m](y,z) = \begin{cases} [S_m(y,z)], & z > 0, \\ [S_m(y,-z)], & z < 0 \end{cases} \tag{49}$$

with

$$[S_m(y,z)] = \frac{a_m}{2\pi\mu k^2} \int_0^\infty \left[-\frac{s^2}{\alpha} \mathrm{e}^{-\alpha z} + \beta \mathrm{e}^{-\beta z} \right] \int_{-1}^{1} \frac{[T(\zeta)]}{\sqrt{1-\zeta^2}} \cos[s(\zeta - y/a_m)] \mathrm{d}\zeta \, \mathrm{d}s, \tag{50}$$

$$[T(\zeta)] = [T_1(\zeta), T_2(\zeta), \ldots, T_N(\zeta)] \tag{51}$$

with $T_j(\zeta)$ being Chebyshev polynomials of the first kind and $\{c\}^m = \{c_1^m, c_2^m, \ldots, c_N^m\}^{\text{T}}$ being the coefficients of Chebyshev polynomial expansion given by Eq. (34).

Accordingly, the pseudo-incident wave along actuator A_n can be obtained by substituting Eq. (48) into Eq. (47) as

$$u_{y_n}^{\text{p}}(y_n, 0) = -\frac{e_{\text{a}}^n E_n}{E_{\text{a}}^n k^{\text{a}}} \sum_{m\neq n}^{N_{\text{a}}} [Q_m(y_n)]\{c\}^m, \tag{52}$$

where

$$[Q_m(y_n)] = -\frac{E_a^n k^a}{e_a^n E_n}[R_m(y_n + y_n^0 - y_m^0, z_n^0 - z_m^0)]. \tag{53}$$

The total incident wave of actuator A_n can then be determined by substituting Eq. (52) into Eq. (43) as

$$u_{y_n}^I(y_n, 0) = -\frac{e_a^n E_n}{E_a^n k^a}\{Q_0(y_n) + \sum_{m\neq n}^{N_a}[Q_m(y_n)]\{c\}^m\}, \tag{54}$$

where

$$Q_0(y_n) = -\frac{E_a^n k^a}{e_a^n E_n} u_{y_n}^0(y_n) \tag{55}$$

with $u_{y_n}^0(y_n)$ being the displacement along the site of actuator A_n due to the initial incident wave u^0.

4.2. Solution of interacting actuators

According to the previously discussed single actuator solution, the Chebyshev polynomial expansion coefficients of actuator A_n, $\{c\}^n = \{c_1^n, c_2^n, \ldots, c_N^n\}^T$, can be determined using Eq. (39) as

$$[A]^n\{c\}^n = \{F\}^n. \tag{56}$$

$[A]^n$ is a known matrix given in Appendix B, and $\{F\}^n$ can be expressed, using Eq. (40), as

$$\{F\}^n = \{f^e\}^n + \{f_I\}^n. \tag{57}$$

in which

$$\{f^e\}^n = \begin{Bmatrix} f_1^n \\ f_2^n \\ \vdots \\ f_N^n \end{Bmatrix}, \qquad \{f_I\}^n = \begin{Bmatrix} f_{I1}^n \\ f_{I2}^n \\ \vdots \\ f_{IN}^n \end{Bmatrix} \tag{58}$$

are the general loads at the following collocation points,

$$\eta_n^j = \eta^j = \frac{y_n^j}{a_n} = \cos\frac{(j-1)\pi}{N-1}, \quad j = 1, 2, \ldots, N, \tag{59}$$

where

$$f_j^n = \frac{\cos\overline{k}_a^n \eta^j}{\sin\overline{k}_a^n}, \qquad f_{1l}^n = -\frac{E_a^n k^a}{e_a^n E_n} u_{y_n}^I(y_n^l, 0) \tag{60}$$

with $u_{y_n}^I$ being the displacement field of the incident wave of actuator A_n, which is given by Eq. (54).

The general force $\{f_I\}^n$ used in Eq. (56) can then be obtained using Eqs. (54) and (58) as

$$\{f_I\}^n = [Q_0]^n + [Q_*]^n\{C\}, \tag{61}$$

where

$$[Q_0]^n = \begin{Bmatrix} Q_0(y_n^1) \\ Q_0(y_n^2) \\ \vdots \\ Q_0(y_n^N) \end{Bmatrix}, \qquad \{C\} = \begin{Bmatrix} \{c\}^1 \\ \{c\}^2 \\ \vdots \\ \{c\}^{N_a} \end{Bmatrix} \tag{62}$$

and

$$[Q_*]^n = \begin{bmatrix} [Q_1(y_n^1)] & [Q_2(y_n^1)] & \cdots & [Q_{N_a}(y_n^1)] \\ [Q_1(y_n^2)] & [Q_2(y_n^2)] & \cdots & [Q_{N_a}(y_n^2)] \\ \vdots & & & \\ [Q_1(y_n^N)] & [Q_2(y_n^N)] & \cdots & [Q_{N_a}(y_n^N)] \end{bmatrix}. \tag{63}$$

By substituting Eqs. (59) and (49) into Eq. (48), the governing equation for solving $\{C\}$ can be obtained as follows:

$$\left\{ \begin{bmatrix} [A]^1 & 0 & \cdots & 0 \\ 0 & [A]^2 & \cdots & 0 \\ 0 & \cdots & \cdots & 0 \\ 0 & 0 & 0 & [A]^{N_a} \end{bmatrix} - \begin{bmatrix} [Q_*]^1 \\ [Q_*]^2 \\ \vdots \\ [Q_*]^{N_a} \end{bmatrix} \right\} \{C\} = \begin{Bmatrix} \{f^e\}^1 + \{Q_0\}^1 \\ \{f^e\}^2 + \{Q_0\}^2 \\ \vdots \\ \{f^e\}^{N_a} + \{Q_0\}^{N_a} \end{Bmatrix}. \tag{64}$$

Eq. (64) indicates that the final result of the original interaction problem can be obtained by solving these linear equations, which can be obtained directly from the analytical solution of the single actuator.

To evaluate the singular behaviour of the interfacial shear stress at the tips of an actuator, we introduce a new parameter: the SSSF, S, defined as

$$\begin{aligned} S_r &= \lim_{y \to a} \left[\sqrt{2\pi(a-y)}\tau(y) \right], \\ S_l &= \lim_{y \to -a} \left[\sqrt{2\pi(a+y)}\tau(y) \right]. \end{aligned} \tag{65}$$

Using Eq. (34), the SSSF at the left and right tips of the actuator can be expressed in terms of the corresponding coefficients of Chebyshev polynomial expansion, c_j, as

$$S_l = p\sqrt{a\pi} \sum_{j=0}^{N-1} (-1)^j c_j, \qquad S_r = p\sqrt{a\pi} \sum_{j=0}^{N-1} c_j \tag{66}$$

which can be expressed in a normalised form as

$$S_l^* = S_l / p\sqrt{\pi a} = \sum_{j=0}^{N-1} (-1)^j c_j, \qquad S_r^* = S_l / p\sqrt{\pi a} = \sum_{j=0}^{N-1} c_j. \tag{67}$$

The SSSF represents the local stress concentration at the tips of the actuator, which has significant effects upon the debonding characteristics of the actuator. The SSSF also governs the load transfer from the actuator to the host structure; a higher SSSF would typically indicate an effective load transfer and control of that structure. However, high values of SSSF may result in interfacial debonding, leading to a reduction in the effective length of the actuator. Thus, there is a trade off between the effectiveness of the actuator and the prevention of failure of the actuator/adaptive structure.

5. Numerical examples

Numerical calculations were carried out for typical examples to investigate the effect of frequency and material constants upon the dynamic behaviour of the actuator.

5.1. Validation of the actuator model

To verify the validity of the present simplified actuator model to predict the interfacial stress distribution, both the current method and the commercial finite element code ANSYS were used to analyse the static shear stress distribution along the boundary of a PZT actuator under an applied electric load. The material constants of the actuator were assumed to be

$$c_{11} = 13.9 \times 10^{10}\ \mathrm{N/m^2}, \quad c_{12} = 6.78 \times 10^{10}\ \mathrm{N/m^2}, \quad c_{13} = 7.43 \times 10^{10}\ \mathrm{N/m^2},$$
$$c_{33} = 11.5 \times 10^{10}\ \mathrm{N/m^2}, \quad c_{44} = 2.56 \times 10^{10}\ \mathrm{N/m^2},$$
$$e_{31} = -5.2\ \mathrm{C/m^2}, \quad e_{33} = 15.1\ \mathrm{C/m^2}, \quad e_{15} = 12.7\ \mathrm{C/m^2},$$
$$\varepsilon_{11} = 6.45 \times 10^{-9}\ \mathrm{C/Vm}, \quad \varepsilon_{33} = 5.62 \times 10^{-9}\ \mathrm{C/Vm}.$$

The matrix is assumed to be an isotropic insulator with

$$E = 70 \times 10^{9}\ \mathrm{N/m^2}, \quad v = 0.33.$$

To simulate the case where the matrix is infinite, a piezoelectric actuator with $a = 10$ mm and $h/2 = 1$ mm (2 mm) embedded in a matrix of 100 mm × 100 mm was considered. The finite element mesh near the actuator for the case where $h = 1$ mm was shown in Fig. 6. Because of the symmetry of the problem, only the right-upper quarter of the structure was considered.

According to the developed actuator model, the effective elastic parameters can be determined to be $q = 5.107$. The interfacial stress distribution from both models are depicted and compared in Fig. 7. These two solutions show fairly good agreement when $y/a < 0.9$ for $v = a/h = 10$. It should be mentioned that in most cases, a/h will be greater than 10. The discrepancy between these two solutions near the tip of the actuator is due to the complex two-dimensional stress distribution in the actuator, which could not be accurately described by the current one-dimensional model. It should be mentioned that by using the current actuator model, all the loads transferred from the actuator to the matrix, including the axial stress at the ends of the actuator, have been represented by the interfacial shear stress, which is singular when the ends of the actuator are approached.

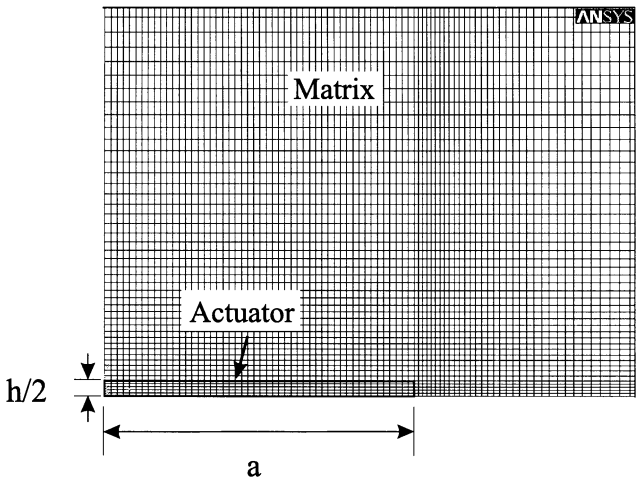

Fig. 6. Finite element mesh used near the actuator.

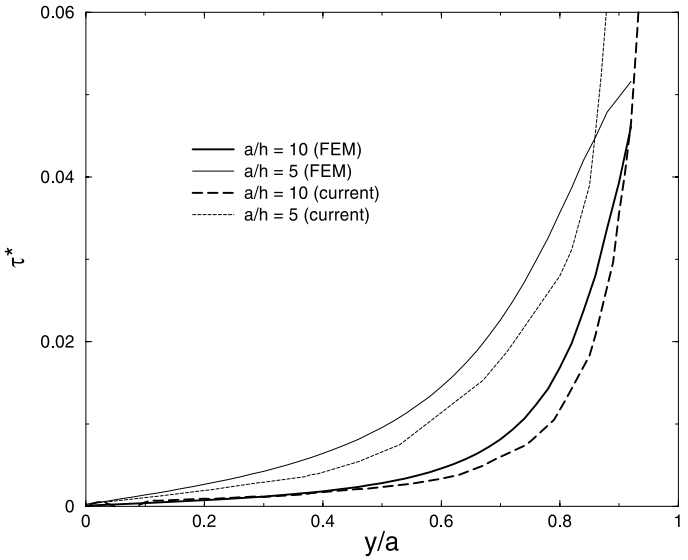

Fig. 7. Shear stress distribution determined by the current model and the finite element method.

5.2. Effect of frequency upon SSSF

Consider the case of an embedded actuator subjected to an applied electric field E_z^0 of frequency ω. Fig. 8 shows the variation of normalised SSSF $S^* = S/p\sqrt{\pi a}$ with the normalised frequency ka for the case where $\rho_a/\rho_H = 1$, $v = 10$. The figure shows the existence of dynamic overshoot, i.e. the dynamic SSSF attains a maximum value which exceeds that corresponding to the static case at a given frequency. This has been found in elastodynamic crack problems (Wang and Meguid, 1997). The result also shows the dramatic effect of the material combination $q = \pi\mu/(1-v)E_a$ upon S^*. Similar to the quasistatic behaviour, in most cases, a lower value of q will result in a higher S^* at the end of the actuator.

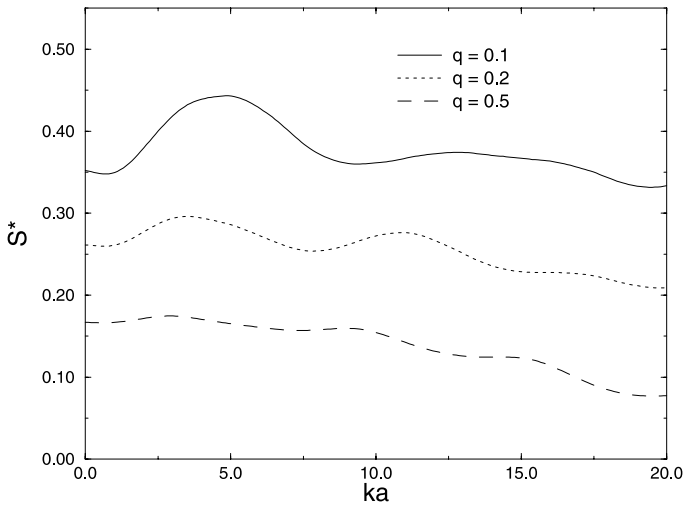

Fig. 8. Dynamic SSSF of an embedded actuator.

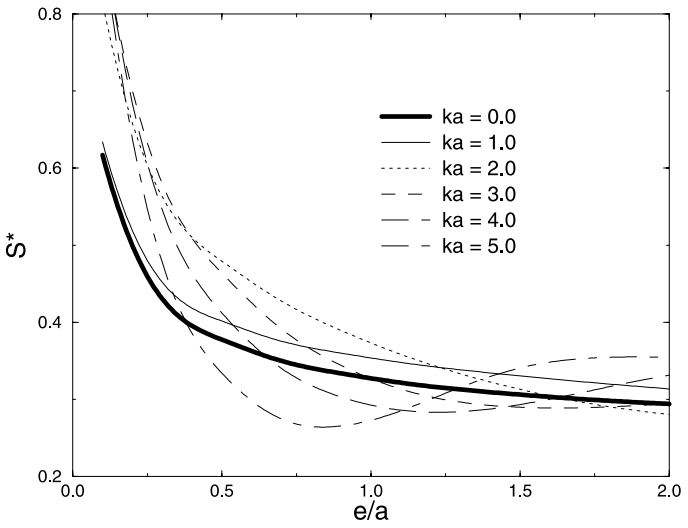

Fig. 9. Dynamic SSSF due to collinear embedded actuators.

5.3. Dynamic interaction between collinear embedded actuators

Fig. 9 shows the variation of the normalised SSSF $S^* = S/p\sqrt{\pi a}$ at the inner tips of two collinear embedded actuators of equal length and thickness for the case where $q = 0.157$ $((1-v)E_a/2\mu = 10)$, $v = a/h = 10$ and $\rho_a/\rho_H = 1$. In this figure, p is given by Eq. (33), a and h are the length and the thickness of the actuators and e is the distance between the interacting tips of the actuators. The two actuators are subjected to the same applied electric field E_z. For the case where the distance between the actuators are larger than a, the interaction between the actuators can be ignored for all the frequencies considered. However, when the actuators are closer, $e < 0.5a$ for example, the interaction between the actuators may result in a significant increase in S^*. It should be noted that it is a common practice to place different actuators in close proximity to achieve high displacement at a specific point of the structure (Ha et al., 1992).

5.4. Dynamic interaction between parallel embedded actuators

Fig. 10 shows the dynamic S^* of two parallel actuators of equal length subjected to the same electric field E_z of frequency ω for the case where $q = 0.157$, $v = 10$ and $\rho_a/\rho_H = 1$. Unlike the collinear case, the interaction between parallel actuators reduces the stress singularity at the ends of the actuators for low frequencies ($ka < 1$). However, for high frequencies ($ka > 1$), the interaction between the actuators amplifies the local stress concentration.

6. Concluding remarks

A general analytical solution is provided to the coupled dynamic electromechanical behaviour of interacting piezoelectric actuators embedded in an elestic medium under plane mechanical and electrical loads. The analysis is based upon the use of a piezoelectric line model of the actuator which reduces the problem to the solution of integral equations in terms of the shear stresses between the actuators and the

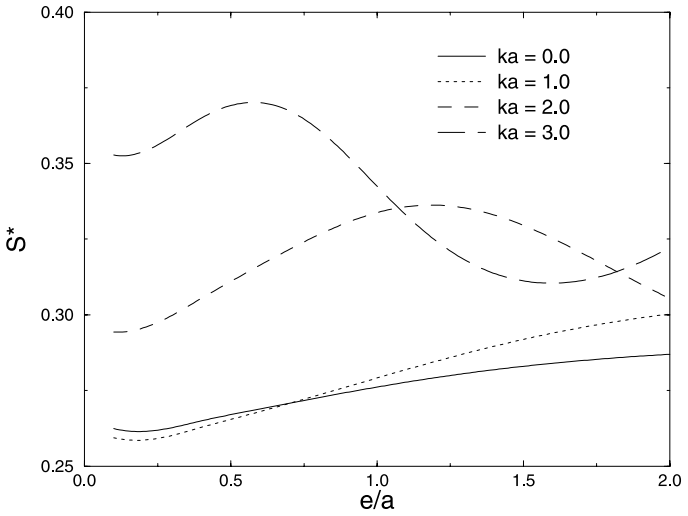

Fig. 10. Dynamic SSSF due to parallel embedded actuators.

matrix. The interaction between different actuators was treated using a pseudo-incident wave method which provides an accurate and reliable solution of the problem by using the single actuator solution as a building block for the interaction model. The newly defined SSSF provides a description of the local stress field around the tip of the actuator. The effect of the shape of the actuators, the material combination and the electromechanical coupling upon the resulting SSSF of the actuators are examined and discussed.

Acknowledgements

This work was supported in part by the Natural Sciences and Engineering Research Council of Canada and in part by the Materials and Manufacturing Centre of Excellence (MMO).

Appendix A. Effective material constants

The mechanical and electrical properties of piezoceramic materials can be described fully by *the equation of motion*

$$\sigma_{ji,j} + f_i = \rho \ddot{u}_i,$$
$$D_{i,i} = 0,$$

Gauss' law
the constitutive equations

$$\{\sigma\} = [c]\{\epsilon\} - [e]\{E\}, \qquad \{D\} = [e]\{\epsilon\} + [\varepsilon]\{E\},$$

where $\epsilon_{ij} = \frac{1}{2}(u_{i,j} + u_{j,i}), \qquad E_i = -V_{,i}.$

In these equations, $\{\sigma\}$ and $\{\epsilon\}$ are the stress and the strain fields, f_i and ρ are the body force and mass density, while $\{D\}$, $\{E\}$ and V represent the electric displacement, the electric field intensity and the potential, respectively. $[c]$ is a matrix containing the elastic stiffness parameters for a constant electric po-

tential, $[e]$ represents a tensor containing the piezoelectric constants and $[\varepsilon]$ represents the dielectric constants for zero strains.

According to the electroelastic line actuator model, the effective material constants of the actuator model are given by

$$E_a = c_{11} - \frac{c_{13}^2}{c_{33}} \quad \text{plane strain},$$
$$e_a = e_{13} - e_{33}\frac{c_{13}}{c_{33}} \quad \text{plane strain},$$
$$\varepsilon_a = \varepsilon_{33} + \frac{e_{33}^2}{c_{33}} \quad \text{plane strain},$$

where the direction of polarization is designated as being the z-axis.

Appendix B. Single actuator solution

The matrices used in Eq. (39) for solving single embedded actuator problem are given by

$$A_{lj} = \frac{\pi}{2(1-\nu)}\frac{\overline{k}_a}{\overline{k}^2}\int_0^\infty P_j^1(\overline{s},\eta^l)\left(\overline{\beta} - \frac{\overline{s}^2}{\overline{\alpha}}\right)\mathrm{d}\overline{s} - qv\int_{\cos^{-1}\eta^l}^{\pi}\sin[\overline{k}_a(\cos\theta-\eta^l)]\cos(j\theta)\mathrm{d}\theta + \pi qv \times \frac{\cos[\overline{k}_a(\eta^l+1)]}{\sin 2\overline{k}_a}P_j^2.$$

The corresponding matrix used in Eq. (48) is given by

$$A_{lj}^n = \frac{\pi}{2(1-\nu)}\frac{\overline{k}_a^n}{\overline{k}^2}\int_0^\infty P_j^1(\overline{s},\eta^l)\left(\overline{\beta}_n - \frac{\overline{s}^2}{\overline{\alpha}_n}\right)\mathrm{d}\overline{s} - q_n v_n\int_{\cos^{-1}\eta^l}^{\pi}\sin[\overline{k}_a^n(\cos\theta-\eta^l)]\cos(j\theta)\mathrm{d}\theta + \pi q_n v_n \times \frac{\cos[\overline{k}_a^n(\eta^l+1)]}{\sin 2\overline{k}_a^n}P_j^2,$$

where P_j^1 and P_j^2 are given by Eq. (37) and η^l are the collocation points along the actuators given by Eq. (38).

References

Achenbach, J.D., 1973. Wave propagation in elastic solids. North-Holland, Amsterdam.

Benveniste, Y., 1992. The determination of the elastic and electric fields in a piezoelectric inhomogeneity. Journal of Applied Physics 72, 1086–1095.

Crawley, E.F., de Luis, J., 1987. Use of piezoelectric actuators as elements of intelligent structures. AIAA Journal 25, 1373–1385.

Crawley, E.F., Anderson, E.H., 1990. Detailed models of piezoelectric actuation of beams. Journal of Intelligent Material Systems and Structures 1, 4–25.

Deeg, W.F., 1980. The analysis of dislocation, crack and inclusion problems in piezoelectric solids. Ph.D. Dissertation, Stanford University.

Disch, J., Lesieutre, G., Koopmann, G., Davis, C., 1995. Inertial piezoceramic actuators for smart structures. SPIE 2447, 14–25.

Dunn, M., Taya, M., 1993. Micromechanical predictions of the effective electro-elastic moduli of piezoelectric composites. International Journal of Solids and Structures 30, 161–175.

Gandhi, M.V., Thompson, B.S., 1992. Smart materials and structures. Chapman & Hall, London.

Ha, S.K., Kerlers, C., Chang, F.K., 1992. Finite element analysis of composite structures containing distributed piezoelectric sensors and actuators. AIAA Journal 30, 772–780.

He, M.-Y., Suo, Z., McMeeking, R.M., Evans, A.G., Lynch, C.S., 1994. The mechanics of some degradation mechanisms in ferroelectric ceramic actuators. SPIE 2189, 344–356.

Im, S., Atluri, S.N., 1989. Effects of a piezo-actuator on a finite deformation beam subjected to general loading. AIAA Journal 27, 1801–1807.

Jain, A.K., Sirkis, J.S., 1994. Continuum damage mechanics in piezoelectric ceramics, adaptive structures and composite materials: analysis and application. ASME AD 45/MD 54, 47–58.

Lin, M.W., Rogers, C.A., 1993a. Modeling of the actuation mechanism in a beam structure with induced strain actuators. In: Proceedings of AIAA/ASCE/ASME/ASC 34th Structures, Structural Dynamics and Materials Conference, AIAA Inc., Washington, DC, Part VI, 3608–3617, La Jolla, CA, 19–22, April.

Lin, M.W., Rogers, C.A., 1993b. Actuation response of a beam structure with induced strain actuators. Adaptive Structures and Material Systems AD 35, 129–139.

Pak, Y.E., 1990. Crack extension force in a piezoelectric material. Journal of Applied Mechanics 57, 647–653.

Sosa, H.A., 1991. Plane problems in piezoelectric media with defects. International Journal of Solids and Structures 28, 491–505.

Suo, Z., Kuo, C.M., Barnett, D.M., Wills, J.R., 1992. Fracture mechanics for piezoelectric ceramics. Journal of Mechanics and Physics of Solids 40, 739–765.

Varadan, V.K., Wu, Z., Bao, X.-Q., Varadan, V.V., 1993. Light weight robot using piezoelectric motor, sensor and actuator. Adaptive Structures and Material Systems AD 35, 141–148.

Wang, X.D., Meguid, S.A., 1997. Diffraction of SH-wave by interacting matrix homogeneity. ASME Journal of Applied Mechanics 64, 568–575.